RSC Advances

PAPER

View Article Online
View Journal | View Issue



Cite this: RSC Adv., 2014, 4, 57329

# Filamentous virus decoration with gold nanoparticles: global fingerprints of bionanocomposites acquired with SERS†

D. Montalvan-Sorrosa,[a] J. L. González-Solis,[b] J. Mas-Oliva[c] and R. Castillo*[a]

Received 17th September 2014
Accepted 22nd October 2014

DOI: 10.1039/c4ra10656c

www.rsc.org/advances

New construction blocks for nanomaterials have been found in nature itself: viruses. Synthetic methods to modify them are relevant for bionanomaterials design. In this paper, a method is presented that takes advantage of the natural functional groups in the fd virus structure to decorate them with gold nanoparticles. The method employs a bioconjugation reaction in which cysteine molecules are appropriately bonded, mediated by carbodiimides, to carboxyl and amine groups in the virus capsid proteins. fd virus with one gold nanoparticle at the tip end and gold nanowire-like structures were obtained. We can discriminate the different synthesized structures, using surface enhanced Raman spectroscopy in conjunction with principal component analysis. The general procedure developed here is a promising tool to determine how viruses are modified after a bioconjugation reaction.



## Introduction

Nanotechnology has recently found new construction blocks in biology, such as short peptides, complex proteins, lipidic membranes, and more recently amyloid fibrils and viruses.[1] Applications of these new supramolecular building blocks have shifted the traditional top-down approach for nanostructure design to a new bottom-up one.[2] Probably, the most remarkable property of these building blocks is self-assembly, which can be successfully exploited for the development of new bionanocomposites. Among biological structures, viruses have played an important role in various nanotechnological developments including biosensing,[3] therapeutics,[4] drug delivery,[5] and energy storage.[6] Reproduction of viruses is genetically controlled and then practically monodisperse. Using a specific host, they can be grown in good yield. Their size can range from a few nanometers to ~400–1000 nm; they are easily observable by Transmission Electron Microscopy (TEM).[7] In addition, viral proteins can be modified using genetic engineering[8] or chemical bioconjugation methods.[9]

In chemical bioconjugation, virus particles are viewed as chemical reagents; they can be added to conventional reaction mixtures available in any organic chemistry lab. Viral surface segments exposed to the solvent are able to react with other biomolecules due to the presence of functional groups such as carboxyl groups (aspartic and glutamic acids, or terminal carboxyls), primary amines (lysine or terminal amines), hydroxyls (tyrosines), thiols (cysteines), and to a lesser extent, the guanidine group from arginine.[1] Typical examples of chemical bioconjugation methods include the Cu(I)-catalyzed azide-alkyne cycloaddition (CuAAC),[10] and the use of functional cross-linkers such as EDC (1-ethyl-3-(3-dimethylaminopropyl)-carbodiimide) and NHS (*N*-hydroxysuccinimide).[1]

### fd virus

The fd bacteriophage is a single chain DNA filamentous virus 800–1000 nm in length and 6 nm in diameter. The capsid is formed by five different proteins: three to five copies of protein III and VI on one end, proteins VII and IX on the other, and approximately 2700 copies of the major coat protein VIII (pVIII). pVIII is a 50 amino acid α-helix assembled as fish scales protecting the DNA[11] and forming the capsid tubular structure (see Fig. 1). Only recently, this virus has been used for bionanocomposite production, unlike its closest relative the M13 virus, which has been widely used in molecular biology and nanotechnology.[12] The fd virus has been widely used as a model to study colloidal systems of semi-rigid rod-like particles forming fluids embedded with threadlike structures[13] and liquid crystals.[14] Filamentous structures have been useful in the design of nanowires as in the case of actin, amyloid fibrils, and rod-like viruses. All of these structures can be metallized by different methods to obtain metal nanowires.[15] In particular, filamentous M13 and fd viruses can be used as a template for obtaining gold bionanocomposites.[16,17]

[a]Instituto de Física, Universidad Nacional Autónoma de México, P. O. Box. 20-364, D. F. 01000, Mexico. E-mail: rolandoc@fisica.unam.mx

[b]Centro Universitario de los Lagos, Universidad de Guadalajara, CP 47460, Lagos de Moreno, Jalisco, Mexico

[c]Instituto de Fisiología Celular, Universidad Nacional Autónoma de México, P. O. Box 70-243, D. F., 04510, Mexico

† Electronic supplementary information (ESI) available: Features of SERS spectra obtained with PCA for the different kinds of synthesized bionanocomposites are provided. See DOI: 10.1039/c4ra10656c

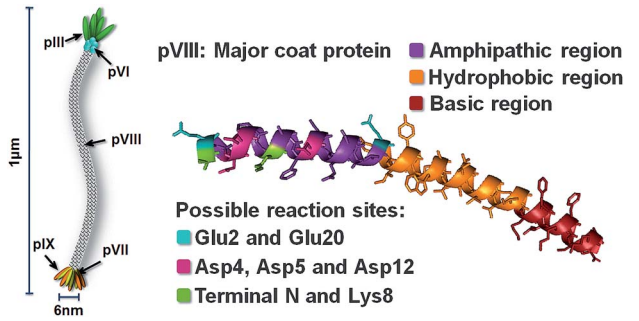


Fig. 1 fd virus scheme showing the viral particle proteins, and the structure of the major coat protein VIII (PDB identifier 1IFD[19]), which is an α-helix composed of 50 amino acids with three principal regions: amphipathic, hydrophobic, and basic (residues involved in DNA charge neutralization).[20] The possible reaction sites are shown in the amphipathic region.

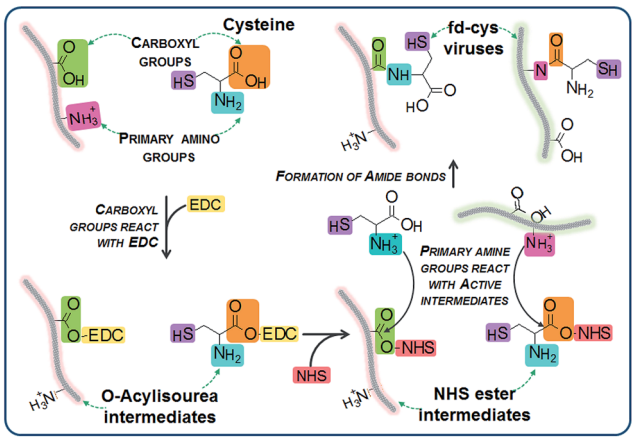


Fig. 2 Main reaction path for virus modification using the cross-link reaction catalyzed with EDC and NHS.

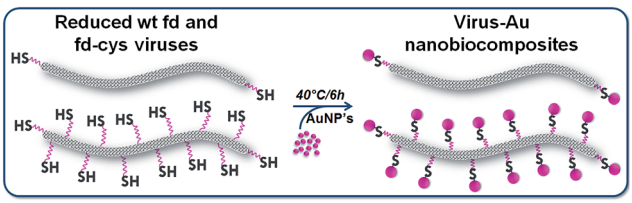


Fig. 3 Decoration of viral particles. After reduction of cysteines (pink wavy lines) free thiol groups are obtained (fd-cys). Addition of AuNPs to the reaction mixture can produce wt fd virus with AuNPs preferentially attached to the tip ends, or gold nanowire-like structures (fd-cys-AuNP).

The fd virus can be chemically modified due to the functional groups present in each coat protein VIII, such as carboxylic acids (Glu2, Glu20, Asp4, Asp5 y Asp12), and primary amines (Lys8 and terminal amine).[18] On the other hand, the high affinity of sulfur atoms to react with gold can play an important role to bond amino acids, such as cysteine and methionine, to gold nanoparticles (AuNPs).[17] However, the number of cysteine amino acids in viral capsids is relatively low; fd virus has just 6 cysteines in each pIII protein, and one for each protein VI, VII and IX. Therefore, there are approximately 35 cysteine groups in one end of the virus, and 6–10 in the other one. pVIII protein does not have any amino acids with sulfur, and the introduction of them by genetic engineering may alter the appropriate protein folding. As a consequence, chemical bioconjugation is an attractive method to carry out surface modification, because practically any biomolecule can be bonded to any of the many functional groups on these pVIII.

One of the most simple bioconjugation reactions uses the zero-length cross-linker 1-ethyl-3-(3-dimethylaminopropyl) carbodiimide (EDC) and *N*-hydroxysuccinimide (NHS). Here, a primary amine and a carboxylic acid form an amide bond as can be seen in Fig. 2, where the fd virus and cysteine are used as reactants. This reaction was originally developed for labeling proteins, and now it is considered as a classic bioconjugation method.[1] Despite the low specificity of the EDC reaction, it is simple and fast for bioconjugation of amino acids. This method is often used as an initial activation step to functionalize nanoparticles towards biomolecule modification.[1]

## Raman spectroscopy

Although, the ultimate test of any successful bionanoconjugation product is to prove functionality in the desired application, they need to be characterized to find a relationship between structure and function. Bionanomaterial architecture has been studied with a variety of well-developed techniques.[21] One of these is the chemically specific Raman spectroscopy. Bands (peaks) in the Raman spectrum are characteristic of specific molecular vibrations providing molecular structural fingerprints.[22] Although Raman scattering spectra provide a lot of information on biological samples, it is an inefficient process because the scattering cross-sections are very low; $\sim 10^{-12}$ to $10^{-14}$ orders of magnitude below the fluorescence cross-sections. Thus, to overcome these problems and to achieve high sensitivity, nanostructured surfaces or noble metal nanoparticles are incorporated in biological samples; scattered intensity is strongly enhanced due to plasmon resonances. This Surface Enhanced Raman Spectroscopy (SERS) has proven to be a very effective technique, where detection sensitivity can be improved by 6 to 10 orders of magnitude compared to conventional Raman spectroscopy.[23,24] SERS produces a spectrum that contains many peaks, some of which are particularly enhanced. Each one of these peaks contains useful biochemical information on the sample.

## Principal component analysis

A statistical method such as the Principal Component Analysis (PCA) is needed to extract as much information as possible from the data. PCA is a linear algebra standard procedure that reduces a complex data set with many peaks to a set of lower orthogonal dimensions, the so-called Principal Components (PCs), with negligible loss of information. In many cases, only the largest PCs are necessary for identifying patterns in data and to highlight differences. This depends on the PCs contribution

 

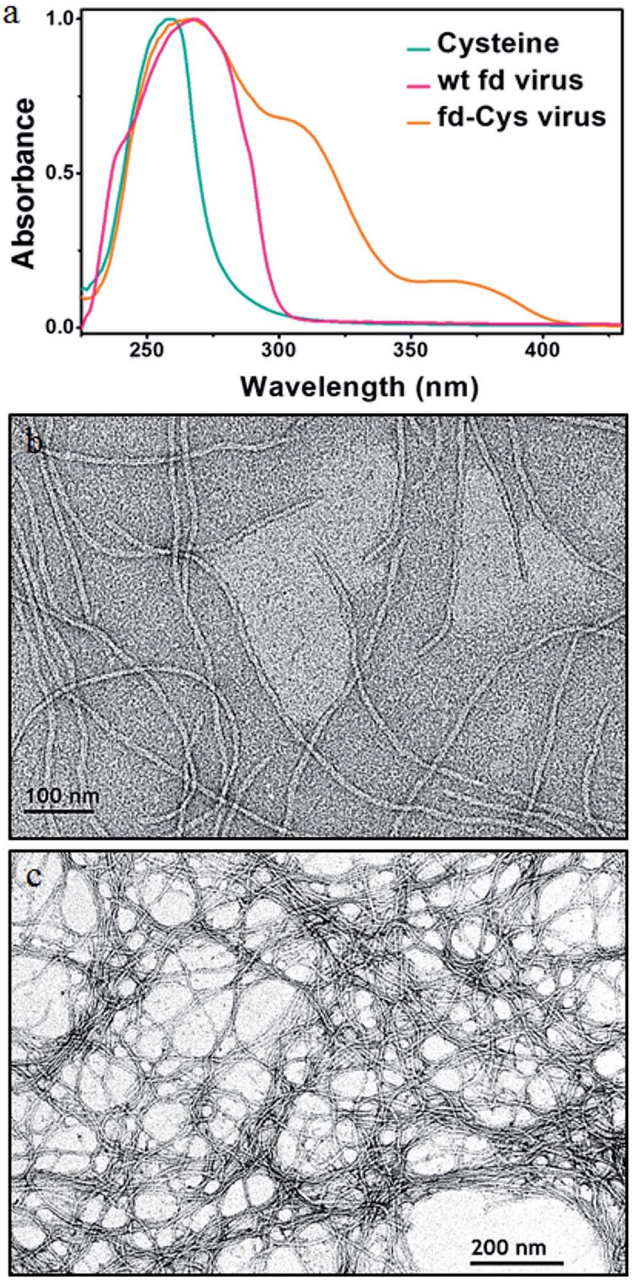


Fig. 4 (a) Ultraviolet spectra of aqueous suspensions of wt fd virus, fd-cys virus, and cysteine in aqueous solution. Electron micrographs of (b) wt fd virus and (c) fd-cys virus.

to the total variance. PCA has been successfully applied in the biomedical area to analyze spectroscopic data from samples in different pathologies.[25–27]

The present paper has two objectives. First, to report the synthesis of bionanocomposites made from the fd virus and AuNPs. A cross-link reaction catalyzed by EDC and NHS is first used to introduce cysteine molecules in the capsid proteins of the virus. Wild-type fd (wt fd) and fd-cysteine (fd-cys) viruses are then bonded to AuNPs. As a result, wt fd with a gold nanoparticle at one tip end and nanowire-like structures are produced. The bionanocomposites are characterized by transmission electron microscopy (TEM), Raman, and SERS. Second, to use PCA to discriminate the main differences among the complex SERS spectra of the modified viruses. The results suggest that this statistical procedure applied to SERS could be a powerful tool for characterizing the different products during bionanocomposite production.

## Results and discussion

Cysteine molecules were introduced along the viral particle to obtain fd-cys viruses, using the reaction catalyzed by carbodiimides discussed above. The conjugation occurs mainly in protein pVIII because it is the most abundant protein in the capsid (Fig. 3).

When UV spectra of cysteine, fd-cys, and wt fd viruses are compared, they differ. The wt fd and fd-cys viruses are red-shifted as compared to cysteine in solution (Fig. 4a), and the UV spectrum of the fd-cys virus has two more peaks than the UV spectrum of the wt fd. Cysteine on the virus surface can induce a slight local unfolding on the neighbor amino acids, particularly important if aromatic amino acid side chains are exposed. Local unfolding is subtle enough to maintain the virus structure (Fig. 4b and c), but enough to be observed in the UV spectrum. As expected, the wt fd and fd-cys viruses cannot be differentiated with TEM (Fig. 4b and c).

Sulfur containing molecules such as thiols and disulfides present a very high affinity for Au surfaces, in particular to those of gold nanoparticles.[28] Nevertheless, we found that when cysteines in the fd-cys virus form disulfide bonds, AuNPs do not bond easily to the viruses. Thus, the disulfide bonds must be previously reduced with $NaBH_4$ to form thiol groups (S–H) in a $N_2$-atmosphere to avoid oxidation.[29] After eliminating the reducing agent with dialysis, freshly prepared AuNPs were added under stirring to the virus suspension, to form the bionanocomposites. In addition, the wt fd virus without cysteine functionalization can also be bonded to the AuNPs at the tip ends due to the native thiol groups (Fig. 3). Actually, AuNPs were attached just to one end tip.

The TEM images of Fig. 5 show the formation of two different kinds of synthesized bionanocomposites after the reaction of the viruses with the AuNPs has taken place: (a) the wt fd virus with a nanoparticle bonded at one tip end of the virus particle (fd-AuNP, Fig. 5a and S1†). Gold nanoparticles are preferentially bonded to one of the tip ends in agreement with the larger number of thiol groups at one end. (b) Gold nanowire-like structures (fd-cys-AuNP, Fig. 5b–d) were obtained by adding AuNPs to previously reduced fd-cys viruses. When only one reaction round was employed to make the fd-cys viruses, a lower amount of AuNPs was attached (Fig. 5b) than when two reaction rounds were employed (Fig. 5c and d).

Although the AuNPs along the viruses are very close together in some cases, they do not present long connected segments. Employing more rounds to attach a greater amount of cysteines on the virus capsid would most likely increase the linear density of the bonded AuNPs. It is important to note that isolated decorated fd-cys-AuNP viruses were not observed at all; they

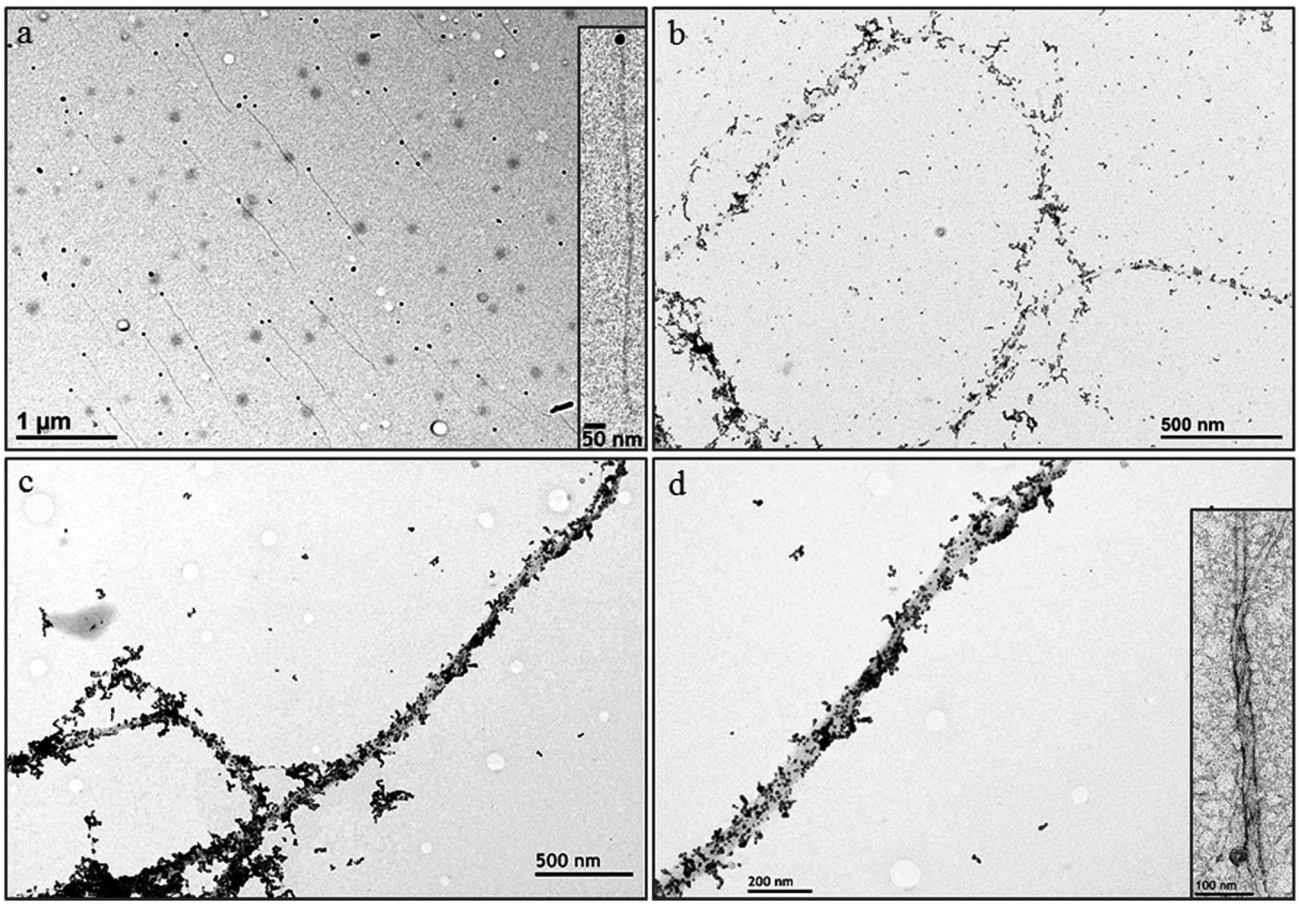


Fig. 5 Electron micrographs of the bionanocomposites. wt fd virus decorated with 15 nm AuNPs at one tip end (a); inset: a decorated wt fd virus at higher magnification. fd-cys-AuNP after one reaction round to obtain the fd-cys viruses (b), and after two reaction rounds to obtain the fd-cys viruses (c) and (d). AuNP diameter = 5 nm. Inset in (d) shows a braided structure made of fd-cys viruses after reduction with $NaBH_4$.

were always forming bundles. Bundle formation occurs prior to the AuNP addition, and it is probably due to the reducing agent ($NaBH_4$), which opens the disulfide bonds inducing cross-linking among fd-cys viruses (inset Fig. 5d). It is not clear which mechanism leads to lateral aggregation of filamentous structures, as in other processes of virus metallization;[30–32] although, it has been argued that divalent ions might be involved.[17]

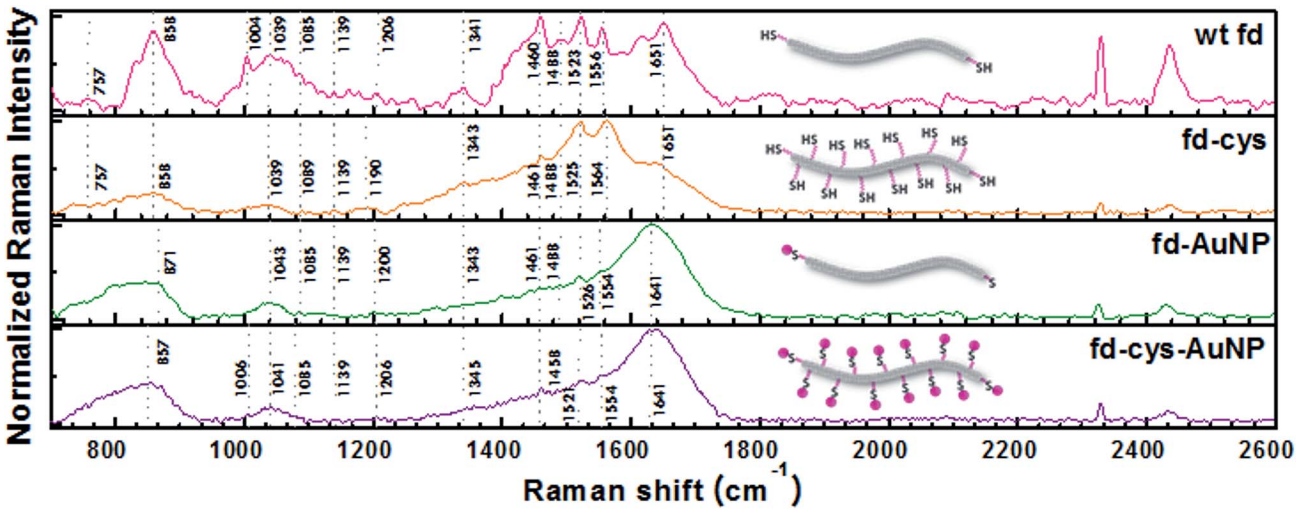


Fig. 6 Average SERS spectra for wt fd virus, fd-cys, fd-AuNP, and fd-cys-AuNP (gold nanowire-like structures).

 

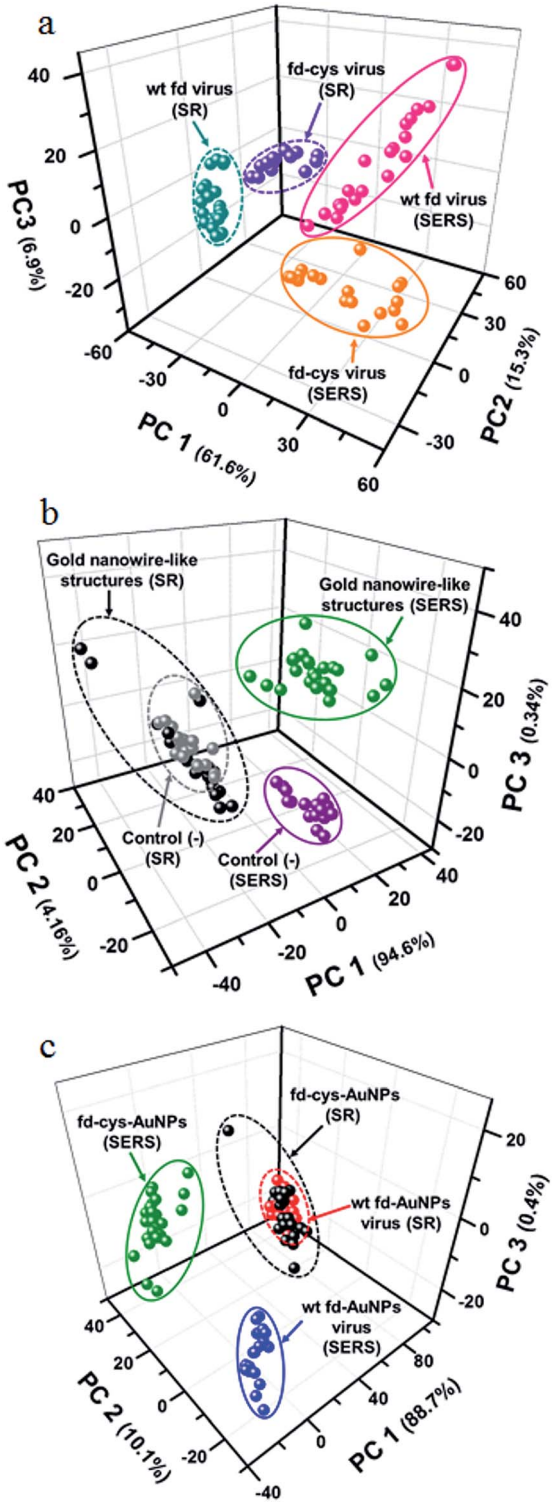


Fig. 7 Three-dimensional plots of the first three largest principal components with their percentage contribution to the total variance (in parenthesis) obtained from SR (enclosed by a dotted line) and SERS (enclosed by a continuous line) for different sets of viruses. (a) Comparison between wt fd and fd-cys viruses. (b) Comparison between the gold nanowire-like structures and the negative control (–). (c) Comparison between the nanowire-like structures and the viruses with an AuNP at one tip end. Total explained variance by the PCs: (a) 83.8%, (b) 99.1%, (c) 99.2%.

Standard Raman (SR) spectra of the modified viruses are not as useful for characterization as SERS, because some distinctive peaks are enhanced in the latter (see Fig. S2†). Fig. 6 presents averaged SERS spectra obtained by adding 30 nm AuNPs to the aqueous suspensions of wt fd virus and bionanocomposites developed in this work. Raman enhancement due to the small AuNPs attached is negligible; larger NPs are needed to get a significant enhancement.

The position of the characteristic Raman peaks previously reported for the wt fd virus[33] are also observed; they are indicated with dotted lines. The spectra of the wt fd virus and the modified ones are different. The most significant differences are observed in two regions of Raman shifts: 700–1200 $cm^{-1}$ and 1400–1650 $cm^{-1}$. However, peaks related to thiol groups are not intense enough to be identified as they become lost in the signal coming from a large number of low-intensity peaks. On the other hand, it can be appreciated that the spectra of fd-Au and fd-cys-Au are relatively similar, and it is difficult to differentiate them. Nevertheless, as will be shown below, PCA reveals hidden patterns and highlights the differences between these spectra.

Fig. 7a presents three-dimensional plots for the first three principal components (PC1, PC2, and PC3) obtained from SR and SERS for sets coming from wt fd and fd-cys viruses; each point corresponds to a particular spectrum in the set. In these plots, four well-differentiated groups emerge. Regardless of whether SR or SERS is employed, PCA differentiates the spectra of wt fd and fd-cys. However, PCA points out the difference between SR and SERS spectra. The plot of the first principal component, PC1, as a function of the Raman shift (Fig. 8), reveals the most important differences between the virus SERS spectra. The observed differences in Fig. 8 are mainly concentrated in the region between 2400 and 2600 $cm^{-1}$, which are related to the stretching of S–H bonds.[34] The main differences are observed at 2462, 2578, 2536, 2549, 2569, and 2588 $cm^{-1}$ (Fig. 8) and are probably related to the introduced amino acid cysteines.

Fig. 7b presents three-dimensional plots for the first three principal components obtained from SR and SERS of the nanowire-like virus sets. We have also included a negative control that was made by adding gold nanoparticles (5 nm) to non-reduced fd-cys viruses; we do not expect them to react, because almost certainly most of the thiol groups in the fd-cys virus are forming disulfide bonds. It is important to note that only when SERS is used, the gold nanowire-like structures and negative control spectra PCs form groups that are far apart from each other; so they can be differentiated. In the same way, Fig. 7c shows that employing SERS, in conjunction with PCA, enables the spectra from fd-AuNP and gold nanowire-like viruses to be separated in a clear way. In contrast, by just using SR, the spectra from both types of viruses cannot be differentiated. It is possible that using a complementary multivariate analysis method, such as Discriminant Function Analysis (DFA), the recognition of patterns inside apparently similar groups could be improved using SR spectra alone.[35]

As mentioned above, it is quite complicated to note the differences between the SERS spectra corresponding to

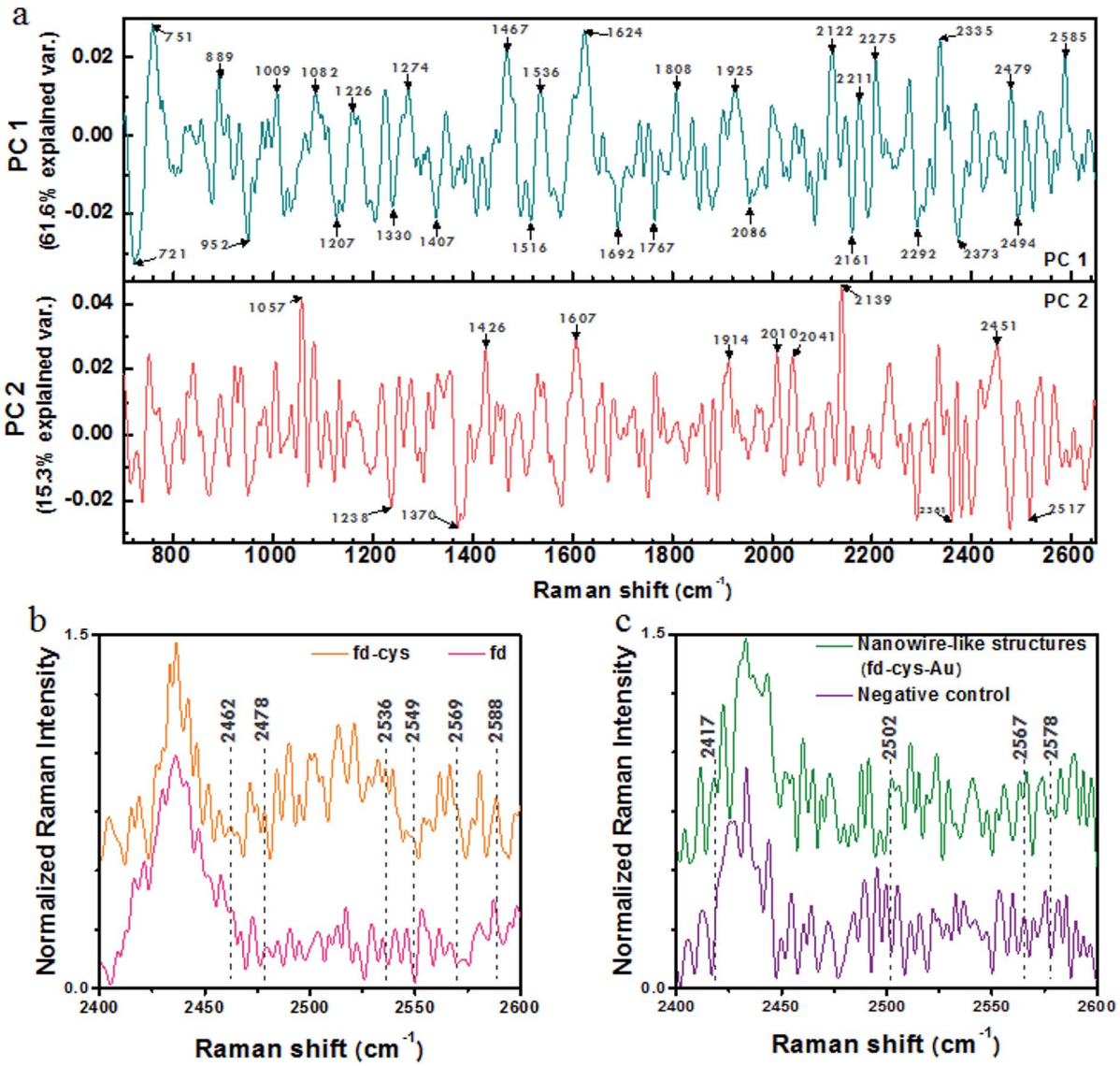


Fig. 8 Main spectra differences. (a) PC1 and PC2 values given by PCA *vs.* the Raman shift for wt fd and fd-cys virus SERS spectra. Peaks with arrows correspond to the main differences between both spectra. Main differences of the sulfur groups in the average SERS spectra between: (b) wt fd and fd-cys virus, and (c) gold nanowire-like structures and the negative control. Vertically displaced to help visualization.

different types of viruses with the naked eye. PCA helps to determine the major differences between the spectra. In Fig. 8a, we present an example showing PC1 and PC2 as a function of the Raman shift that shows the main differences between the wt fd and fd-cys virus' spectra. These differences correspond mainly to the vibrations of amide bonds and sulfur related groups; specific vibration modes can be assigned to those peaks (see Table S1†). The $CO_2$ stretching at 1624 $cm^{-1}$ may be attributed to the cysteine carboxyl groups, occurring when amino groups of cysteine reacted with protein pVIII carboxy groups. On the other hand, the peaks at 1226 and 1467 $cm^{-1}$ can be attributed to amines and amides resulting from the bioconjugation of the carboxyl groups of cysteine with pVIII amino groups.

However, there are also vibrations from different functional groups that can contribute to a specific peak as observed in Table S1,† or signals related to trace molecules, as in the case of 1226 $cm^{-1}$. This peak can be related to the amide III, or to the N=N=N stretching of azides coming from the sodium azide in the buffer solution added to prevent microbial growth. Similar plots were also obtained from different sets of spectra (see Fig. S3 and S4, and Tables ST2 and ST3†). The differences in intensities in the original spectra can be retrieved from the main differences given by the PCs, which can be observed in Fig. 8b and c. Here, we present the main differences in the spectra with dotted lines that correspond to S–H bond stretching. Prior to the chemical synthesis, there is no peak for this mode, but it is present after reaction. In Fig. 8b, we present relative Raman intensities for the wt fd and fd-cys viruses for the

 

region 2400–2600 $cm^{-1}$. The same occurs in Fig. 8c for the case of fd-cys-Au nanowire-like structures and the negative control.

## Conclusions

We described a method developed to take advantage of native functional groups located in the fd virus structure for decorating them with gold nanoparticles. In this method, a bioconjugation reaction mediated by carbodiimides was used, where cysteine molecules were appropriately bonded to carboxyl or amine groups in the virus capsid proteins. fd virus with gold nanoparticles at one tip end and gold nanowire-like structures were obtained. The resulting structures were observed with transmission electron microscopy. This bioconjugation reaction on filamentous viruses might be helpful for attaching other metal nanoparticles, such as those made of silver. In addition, the nanoparticles might have different morphologies and sizes allowing a better hot spot design for Raman signal enhancement. These bionanocomposites are used as novel virus-based protein carriers functioning as SERS nanoprobes.[36]

We also described a procedure to discriminate the different synthesized structures using surface enhanced Raman spectroscopy in conjunction with the Principal Component Analysis statistical procedure. In the present case, the inclusion of a statistical method to determine the Raman signatures in biomolecules interacting with inorganic materials during the production of bionanocomposites was useful. This procedure showed that chemically modified viruses can be differentiated, providing a fast and promising strategy to characterize different bionanocomposites produced along synthetic pathways.

## Experimental section

### Virus production

The fd production is based on a method for M13 growth and purification.[37] fd virus was produced using *Escherichia coli* XL1-Blue strain as the host bacteria. A large batch of bacteria was obtained and infected with fd virus (ATCC 1566-B2). After a few hours, bacterial cells were separated using low-speed centrifugation. Afterwards, the virus was concentrated using polyethylene glycol and subsequent ultracentrifugation. A pellet was obtained and suspended. This suspension was extensively dialyzed against 20 mM Tris–HCl buffer at pH = 8.15. Sodium azide was added to prevent bacterial growth.

### Bioconjugation with cysteine

A 300 mM cysteine solution and a 15 mg $mL^{-1}$ fd virus suspension were both prepared in a 20 mM sodium phosphate buffer at pH = 7.2. 9 mL of the cysteine solution were mixed with 1 mL of the fd suspension (final concentration ~1.5 mg $mL^{-1}$). Then, 4 mmol of 1-ethyl-3-(3-dimethylaminopropyl) carbodiimide (EDC) and 2 mmol of *N*-hydroxysuccinimide (NHS) were added, and quickly mixed. The reaction was performed at room temperature for 6 h under $N_2$ atmosphere. The suspension pH was maintained between 5 and 5.5. The modified virus suspension was extensively dialyzed against 20 mM Tris–HCl buffer at pH = 8.15. The dialyzed suspension was used again for a second bioconjugation round with cysteine. In this case, cysteine was first solubilized in a small volume of the phosphate buffer, and then added to the virus suspension. The previous reaction and purification procedures were repeated for a second time. Finally, the modified virus was stored in containers under $N_2$ at 5 °C.

### Gold nanoparticle (AuNP) synthesis

The synthesis of 30 nm AuNPs was achieved using citrate as the reducing agent at 100 °C following the method of Frens.[38] 30 mL of gold hydrochloride (Sigma) solution was prepared with ultrapure water and heated up. When this solution started to boil, it was vigorously mixed with 30 mL of a preheated sodium citrate (Sigma) solution. Sodium citrate and gold hydrochloride were prepared at the same concentration. For 5 nm AuNP synthesis, 10 mL of the gold hydrochloride solution was mixed with 10 mL of the sodium citrate solution. Then, 1.2 mL of 50 mM $NaBH_4$ was quickly added and stirred for 20 min at room temperature. For both AuNP syntheses, when the suspension color does not change anymore (~20 min), the suspension at room temperature is dialyzed against sterile distilled water.

### fd decoration with AuNPs

1 mmol of $NaBH_4$ was added to the virus suspensions to reduce the disulfide bonds present in both the wt fd and the modified virus structures. The mixtures were incubated at 37–40 °C with gentle agitation for 30 min taking care of the $H_2$ production in this step; an extraction hood is needed. Suspensions were immediately dialyzed against 20 mM Tris–HCl buffer at pH = 8.15 during 1 h with buffer replacements every 10 min; oxygen-free $N_2$ gas was bubbled into the dialysis buffer to avoid thiol oxidation. After dialysis, 0.5 mL of the suspension was mixed with the same volume of a 5 nm AuNP suspension. The samples were incubated at 40 °C with agitation for 6 h.

### Transmission electron microscopy (TEM)

Diluted suspensions of virus were deposited on carbon-coated TEM grids and stained with 2% uranyl acetate. The negatively stained samples were observed with a TEM JEM-1200EX11 (JEOL, Japan) and analyzed with the DigitalMicrograph™ 2.3 software.

### Ultraviolet spectrophotometry

The UV-Vis spectroscopy measurements were performed with a DR 5300 UV-Vis spectrophotometer (HACH Company, USA).

### Raman spectroscopy

Raman spectra were obtained using a diode-pumped solid state laser (532 nm) DXR Raman microscope (Thermo Scientific, USA). For SERS measurements, a suspension with 30 nm AuNPs was added to the virus samples. The mixtures were vigorously shaken, and then kept at room temperature for 12–24 h. For SR and SERS measurements, 0.5 mL of the sample was placed on a

$CaF_2$ recipient in the microscope holder. A minimum of 15 spectra for each sample were collected; each with 15 exposition windows of 10 s. For the analysis of the SR and SERS data we used the PCA method. Here, several data matrices were constructed from the raw collected Raman spectra. Columns correspond to the measured intensity spectra, and rows to the specific Raman shifts. Previously, spectra were processed by carrying baseline correction, smoothing and normalization to remove noise. Sample fluorescence was removed with a filter based on the baseline correction with the Asymmetric Least Squares Smoothing Algorithm. Finally, PCA was performed using a MatLab algorithm. The main information was described with the first three principal components. The assignment of functional groups to the relevant peaks in the spectra was based on standard databases for Raman spectra.[39]

## Acknowledgements

We thank B. A. Delgado-Coello, R. Paredes, C. Garza, and S. Ramos for their technical support. Funding from SEP-CONACYT (81081), DGAPA-UNAM (IN 110414), and CONACYT scholarship for D. M.-S. in the Biomedical Sciences Graduate Program at UNAM are gratefully acknowledged.

## Notes and references

1 K. E. Sapsford, W. R. Algar, L. Berti, K. B. Gemmill, B. J. Casey, E. Oh, M. H. Stewart and I. L. Medintz, *Chem. Rev.*, 2013, **113**, 1904–2074.
2 S. Howorka, *Curr. Opin. Biotechnol.*, 2011, **22**, 485–491.
3 C. Mao, A. Liu and B. Cao, *Angew. Chem., Int. Ed.*, 2009, **48**, 6790–6810.
4 R. Farr, D. S. Choi and S.-W. Lee, *Acta Biomater.*, 2014, **10**, 1741–1750.
5 D. Ghosh, A. G. Kohli, F. Moser, D. Endy and A. M. Belcher, *ACS Synth. Biol.*, 2012, **1**, 576–582.
6 P.-Y. Chen, X. Dang, M. T. Klug, J. Qi, N.-M. Dorval Courchesne, F. J. Burpo, N. Fang, P. T. Hammond and A. M. Belcher, *ACS Nano*, 2013, **7**, 6563–6574.
7 J. Glasgow and D. Tullman-Ercek, *Appl. Microbiol. Biotechnol.*, 2014, **98**, 5847–5858.
8 M. G. Mateu, *Protein Eng., Des. Sel.*, 2011, **24**, 53–63.
9 S. Ng, M. R. Jafari and R. Derda, *ACS Chem. Biol.*, 2012, **7**, 123–138.
10 M. A. Bruckman, G. Kaur, L. A. Lee, F. Xie, J. Sepulveda, R. Breitenkamp, X. Zhang, M. Joralemon, T. P. Russell, T. Emrick and Q. Wang, *ChemBioChem*, 2008, **9**, 519–523.
11 D. A. Marvin, M. F. Symmons and S. K. Straus, *Prog. Biophys. Mol. Biol.*, 2014, **114**, 80–122.
12 A. Merzlyak and S.-W. Lee, *Curr. Opin. Chem. Biol.*, 2006, **10**, 246–252.
13 E. Sarmiento-Gomez, D. Montalvan-Sorrosa, C. Garza, J. Mas-Oliva and R. Castillo, *Eur. Phys. J. E: Soft Matter Biol. Phys.*, 2012, **35**, 35.
14 Z. Dogic and S. Fraden, *Curr. Opin. Colloid Interface Sci.*, 2006, **11**, 47–55.
15 S. I. Stupp and L. C. Palmer, *Chem. Mater.*, 2014, **26**, 507–518.
16 Y. Huang, C.-Y. Chiang, S. K. Lee, Y. Gao, E. L. Hu, J. De Yoreo and A. M. Belcher, *Nano Lett.*, 2005, **5**, 1429–1434.
17 N. Korkmaz, *Colloids Surf., B*, 2013, **112**, 219–228.
18 Z. Zhang and E. Grelet, *Soft Matter*, 2013, **9**, 1015.
19 D. A. Marvin, *Int. J. Biol. Macromol.*, 1990, **12**, 125–138.
20 W. L. Vos, P. V Nazarov, R. B. M. Koehorst, R. B. Spruijt and M. A. Hemminga, *Trends Biochem. Sci.*, 2009, **34**, 249–255.
21 K. E. Sapsford, K. M. Tyner, B. J. Dair, J. R. Deschamps and I. L. Medintz, *Anal. Chem.*, 2011, **83**, 4453–4488.
22 C. V. Raman and K. S. Krishnan, *Nature*, 1928, **121**, 501–502.
23 S. Chan, S. Kwon, T. Koo, L. P. Lee and A. A. Berlin, *Adv. Mater.*, 2003, **15**, 1595–1598.
24 R. L. Garrell, *Anal. Chem.*, 1989, **61**, 401A–411A.
25 I. Barman, N. C. Dingari, G. P. Singh, R. Kumar, S. Lang and G. Nabi, *Anal. Bioanal. Chem.*, 2012, **404**, 3091–3099.
26 R. Jain, D. Calderon, P. R. Kierski, M. J. Schurr, C. J. Czuprynski, C. J. Murphy, J. F. McAnulty and N. L. Abbott, *Anal. Chem.*, 2014, **86**, 3764–3772.
27 B. Chen, S. Li, J. Li, Z. Guo, Q. Chen and H. Mai, *J. Appl. Phys.*, 2013, **114**, 244702.
28 W. Fritzsche and T. A. Taton, *Nanotechnology*, 2003, **14**, R63–R73.
29 R. E. Hansen and J. R. Winther, *Anal. Biochem.*, 2009, **394**, 147–158.
30 B. Neltner, B. Peddie, A. Xu, W. Doenlen, K. Durand, D. S. Yun, S. Speakman, A. Peterson and A. Belcher, *ACS Nano*, 2010, **4**, 3227–3235.
31 K. N. Avery, J. E. Schaak and R. E. Schaak, *Chem. Mater.*, 2009, **21**, 2176–2178.
32 S.-K. Lee, D. S. Yun and A. M. Belcher, *Biomacromolecules*, 2006, **7**, 14–17.
33 S. A. Overman, D. M. Kristensen, P. Bondre, B. Hewitt and G. J. Thomas, *Biochemistry*, 2004, **43**, 13129–13136.
34 S. W. Raso, P. L. Clark, C. Haase-Pettingell, J. King and G. J. Thomas, *J. Mol. Biol.*, 2001, **307**, 899–911.
35 S. Devpura, J. S. Thakur, S. Sethi, V. M. Naik and R. Naik, *J. Raman Spectrosc.*, 2012, **43**, 490–496.
36 H.-E. Lee, H. K. Lee, H. Chang, H.-Y. Ahn, N. Erdene, H.-Y. Lee, Y.-S. Lee, D. H. Jeong, J. Chung and K. T. Nam, *Small*, 2014, **10**, 3007–3011.
37 J. Sambrook and D. W. Russell, in *Molecular Cloning: A Laboratory Manual*, ed. J. Sambrook and D. W. Russell, Cold Spring Harbor Laboratory Press, Cold Spring Harbor, New York, 3rd edn, 2001, pp. 3.1–3.52.
38 G. Frens, *Nature Phys. Sci.*, 1973, **241**, 20–22.
39 G. Socrates, *Infrared and Raman Characteristic Group Frequencies: Tables and Charts*, John Wiley and Sons Ltd, England, 3rd edn, 2001.

 